EPJ Web of Conferences **73**, 01007 (2014)
DOI: 10.1051/epjconf/20147301007

Brief review on generalized parton distributions

Michel Guidal[a]

Institut de Physique Nucléaire d'Orsay, Orsay, France

Abstract. We briefly review some recent developments in the field of Generalized Parton Distributions (GPDs) and Deeply virtual Compton scattering in the valence region. First steps in the direction of nucleon imaging are presented.

1. Introduction

Forty years after the discovery of quarks in the nucleon, the precise way they compose the nucleon remains a largely unveiled mystery. Why do they remain confined within a 1 fermi cube or so volume? How are they (spatially, momentum, ...) distributed in this volume? How do they contribute to the global properties (charge, magnetism, spin, ...) of the nucleon?

The scattering of high energy leptons is a powerful tool to study the structure of the nucleon in terms of partons (i.e. quarks and gluons) and to answer some of these questions. One can distinguish three general classes of processes: 1/ elastic lepton-nucleon scattering, $lN \to l'N'$, which measures the "Form Factors" (FF) of the nucleon. In a frame where the nucleon goes to the speed of light in a certain direction, the FFs give access, via the equivalent of a Fourier transform on the squared momentum transfer to the nucleon, to the *transverse spatial* $b_\perp$ density of electromagnetic (or axial) charges in the nucleon; 2/ deep inclusive lepton-nucleon scattering $lN \to l'X$, generically called "Deep Inelastic Scattering" (DIS), which measures the "Parton Distribution Functions" (PDFs). The PDFs can be interpreted as the probability to find a parton with a given *longitudinal momentum* fraction x in a nucleon; and 3/ exclusive electron-nucleon scattering $lN \to l'N'(M, \gamma)$, where M stands for a meson and γ for a photon, generically called "Deep Exclusive Scattering" (DES), which accesses the "Generalized Parton Distributions" (GPDs), the subject of this short review. Figure 1 illustrates these processes.

In the quark sector, at QCD leading twist, there are eight GPDs: $H, \tilde{H}, E, \tilde{E}, H_T, \tilde{H}_T, E_T, \tilde{E}_T$. In DVCS and DVMP, due to helicity conservation arguments, only the first four can be accessed at QCD leading twist and they reflect the four independent spin/helicity transitions between the initial and final nucleons/quarks in the "handbag" diagrams of the bottom part of Fig. 1.

GPDs depend on three variables: x, ξ (which is equivalent to the well-known x_B variable used in DIS: $\xi = \frac{x_B}{2-x_B}$) and t, the squared momentum transfer between the inital and final nucleon. At QCD

[a] e-mail: guidal@ipno.in2p3.fr

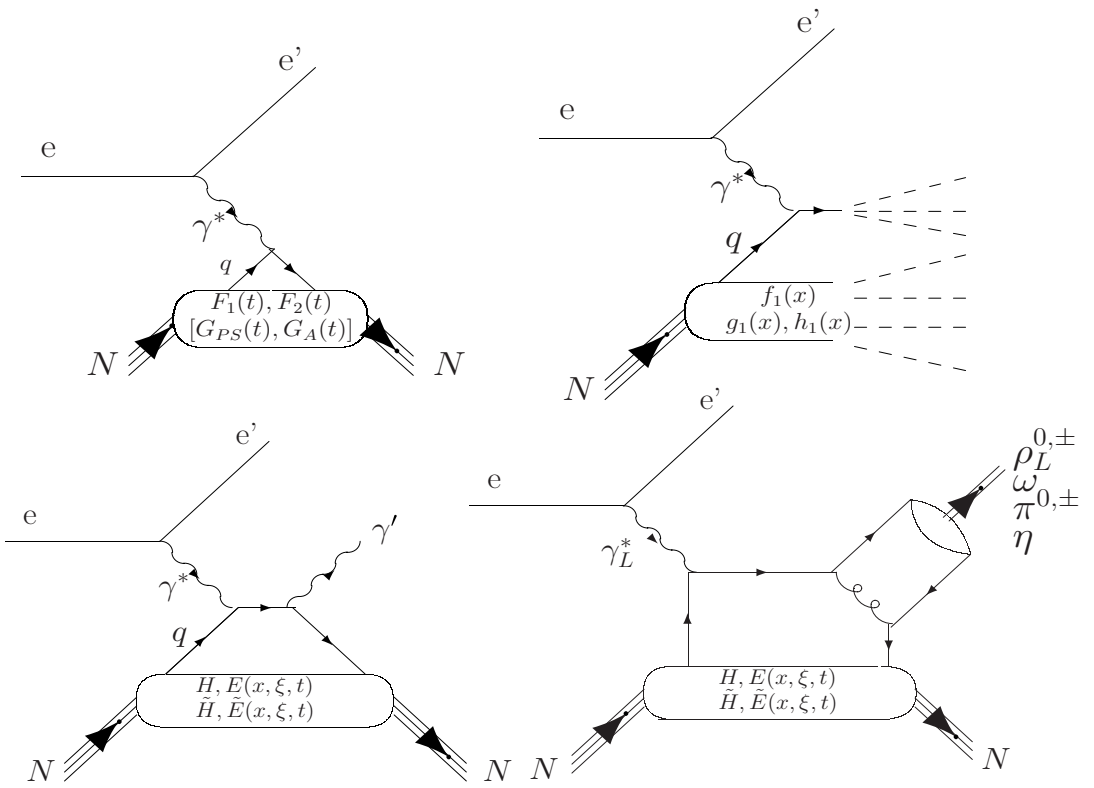

Figure 1. Top left: elastic scattering $lN \to l'N'$ where the complex structure of the nucleon is parametrized in terms of FFs. Top right: deep inelastic scattering $lN \to l'X$ where the complex structure of the nucleon is parametrized in terms of PDFs. Bottom left and right: deep exclusive scattering $lN \to l'(M,\gamma)$ where the complex structure of the nucleon is parametrized in terms of GPDs. Bottom left: "handbag diagram" for Deep Virtual Compton Scattering (DVCS); Bottom right: "handbag diagram" for Deep Virtual Meson Production (DVMP).

leading order, GPDs don't depend on Q^2. In DVCS, the variables ξ and t can be measured, respectively by measuring the scattered lepton and the final photon (or recoil nucleon), but x is not experimentally accessible. It is a "mute" variable which is integrated over, due to the loop in the handbag diagrams (see Fig. 1). The interpretation of these variables is the following: in a frame where the nucleon goes to the speed of light along a certain direction, GPDs represent the probability amplitude of finding a quark in the nucleon with a *longitudinal* momentum fraction $x + \xi$ and of putting it back into the nucleon with a *longitudinal* momentum fraction $x - \xi$ (plus some transverse momentum "kick", which is represented by t). Also, at $\xi = 0$, they can be interpreted as the probability amplitude of finding in a nucleon a parton with *longitudinal* momentum fraction x at a given *transverse* impact parameter $b_\perp$, which is the conjugate variable of t. One sees then how the information contained in a traditional PDF, as measured in DIS, and the information contained in a FF, as measured in elastic lepton-nucleon scattering, are now combined and correlated in the GPD description. In the forward limit ($\xi, t \to 0$), GPDs actually reduce to PDFs and their first x-moment are equal to FFs. Also, their second x-moment gives access to the quark orbital contribution to the nucleon spin.

We refer the reader to the reviews [1–4] on GPDs for details. In this review, due to space constraints, we limit ourselves in the following to recap what are the currently existing DVCS data in the valence

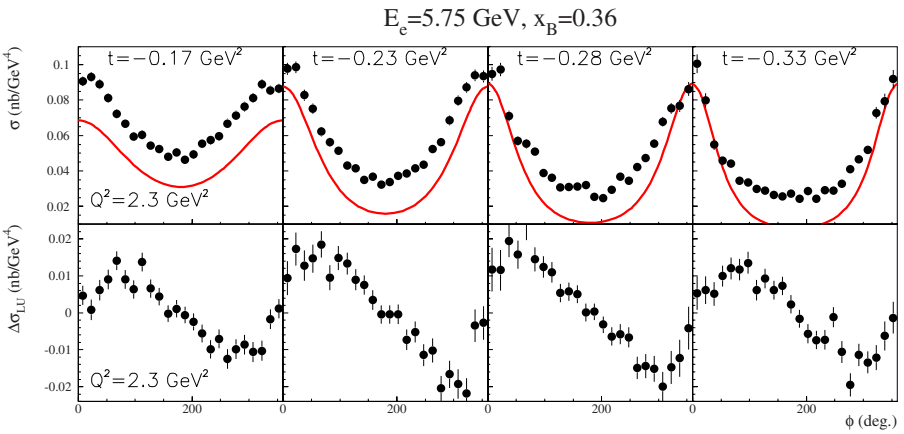

Figure 2. The top row shows the DVCS+BH unpolarized cross sections on the proton, as a function of the ϕ angle, measured by the JLab Hall A collaboration [5]. The red curves show the BH contribution. The bottom row shows the difference of beam-polarized cross section as a function of ϕ for the same kinematics.

region, what GPD information has been extracted from them via recently developped dedicated fitter codes and what first "tomographic" (i.e. x vs $b_\perp$) images of the nucleon begin to emerge.

2. The data

Three experiments have provided these past 10 years DVCS data in the valence region which can lend themselves to a GPD interpretation. These are the Hall A and CLAS experiments from JLab (with a $\approx$ 6 GeV electron beam energy) and the HERMES experiment at DESY (with a $\approx$ 27 GeV electron or positron beam energy).

The Hall A experiment measured the 4-fold beam-polarized and unpolarized differential cross sections $d\sigma/dx_B dQ^2 dt d\phi$, i.e. without any integration over an independent variable, as a function of ϕ (the angle between the leptonic and hadronic plane), for four $-t$ values (0.17, 0.23, 0.28 and 0.33) at the average kinematics: $< x_B >= 0.36$ and $< Q^2 >= 2.3$ GeV^2. The beam-polarized cross sections have also been measured at $< Q^2 >= 1.5$ GeV^2 and $< Q^2 >= 1.9$ GeV^2. The particular shape in ϕ of the unpolarized cross section (red curve in the upper panels of Fig. 2) is due to the Bethe-Heitler (BH) process. Indeed, the $ep \to ep\gamma$ reaction is not purely made of the DVCS process. The latter is accompanied by the BH process, in which the final state photon is radiated by the incoming or scattered electron and not by the nucleon itself. It therefore doesn't really contain any new information on the nucleon structure and the GPDs. It is however rather precisely calculable. In Fig. 2, the difference between the red curve and the data is the contribution of the DVCS process and therefore of the GPDs.

The CLAS collaboration uses a large acceptance spectrometer and has measured the Beam Spin Asymmetry (BSA) of the DVCS process over a broad phase space. Pioneering measurements of the longitudinally polarized target asymmetries (lTSA) have also been published by the CLAS collaboration. These observables are shown in Figs. 3 and 4. There are many new data and observables currently under analysis at JLab and we refer the reader to the proceedings of S. Niccolai in this conference for the latest news.

At higher energies, $x_B \approx 0.1$, the HERMES collaboration has carried out a measurement of ALL independent DVCS observables, except for cross sections: beam spin asymmetries [8, 9], longitudinally polarized target asymmetries [10], transversally polarized target asymmetries [11, 12], beam charge asymmetries [13–15] and all associated beam spin/target spin and spin/beam-charge double

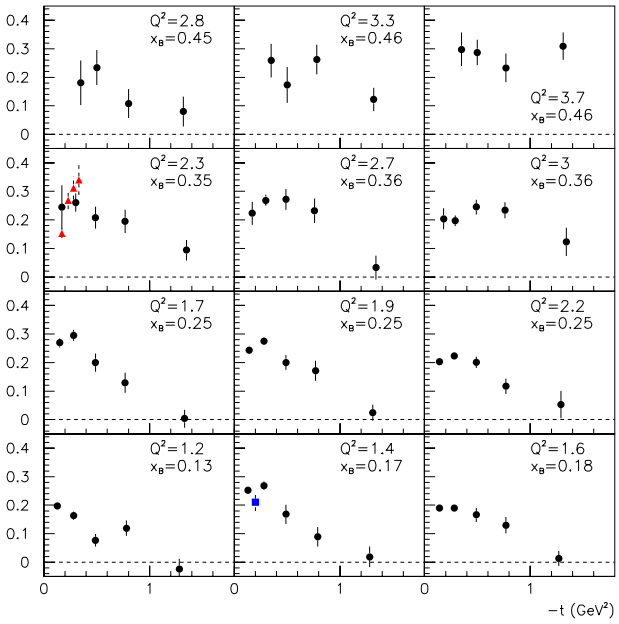

Figure 3. Solid circles: DVCS BSA at $\phi = 90^\circ$ as a function of t for different (x_B, Q^2) bins, as measured by CLAS [6].

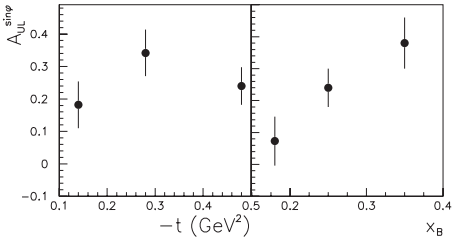

Figure 4. The $\sin(\phi)$ moments of the lTSA [7]. Left: Three $-t$ bins, integrated over x_B; Right: Three x_B bins, integrated over t.

asymmetries. Due to lack of space, we don't show them here but we refer the reader to the proceedings of M. Dueren in this conference.

3. From data to a first attempt at nucleon imaging

The question arises now how to extract the GPD information from the existing DVCS data. These past few years, three groups (D. Müeller and K. Kumericki [16, 17], H. Moutarde [18] and M. Guidal [19–22]) have developped fitting codes and algorithms aimed at extracting the GPD information from the DVCS data. We recall that GPDs depend on three variables: x, ξ and t but that x is not measurable in DVCS. Precisely, the DVCS amplitude is proportional to: $\int_{-1}^{+1} dx \frac{H(x,\xi,t)}{x-\xi+i\epsilon} + ...$ (where the ellipsis stand for similar terms in E, $\tilde{H}$ and $\tilde{E}$). The $\frac{1}{x-\xi+i\epsilon}$ term is the propagator of the quark between the incoming virtual photon and the outgoing photon (see the bottom left patr of Fig. 1). The previous expression can be decomposed into a real and an imaginary part: $PP(\int_{-1}^{+1} dx \frac{H(x,\xi,t)}{x-\xi}) + i\pi H(\xi,\xi,t)$. This means that the maximum information that can be extracted from the experimental data at a given (ξ, t) point is $H(\pm\xi, \xi, t)$, when measuring an observable sensitive to the imaginary part of the DVCS amplitude, and $\int_{-1}^{+1} dx \frac{H(\mp x,\xi,t)}{x\pm\xi}$, when measuring an observable sensitive to the real part of the DVCS amplitude. These quantities are called "Compton form Factors" (CFFs) and will be denoted in the following, respectively, as H_{Im} and H_{Re} (and similarly for E, $\tilde{H}$ and $\tilde{E}$).

Each experimental observable (cross section, BSA, lTSA, etc.) is dominated by a specific CFF or a particular combination of CFFs. Ultimately, with enough observables measured, essentially all CFFs will be accessible. From the limited set of data presented in Sect. 2, with their present accuracy, it has been possible so far to extract constraints on three CFFs: H_{Re}, H_{Im} and $\tilde{H}_{Im}$. In Fig. 5, we show the

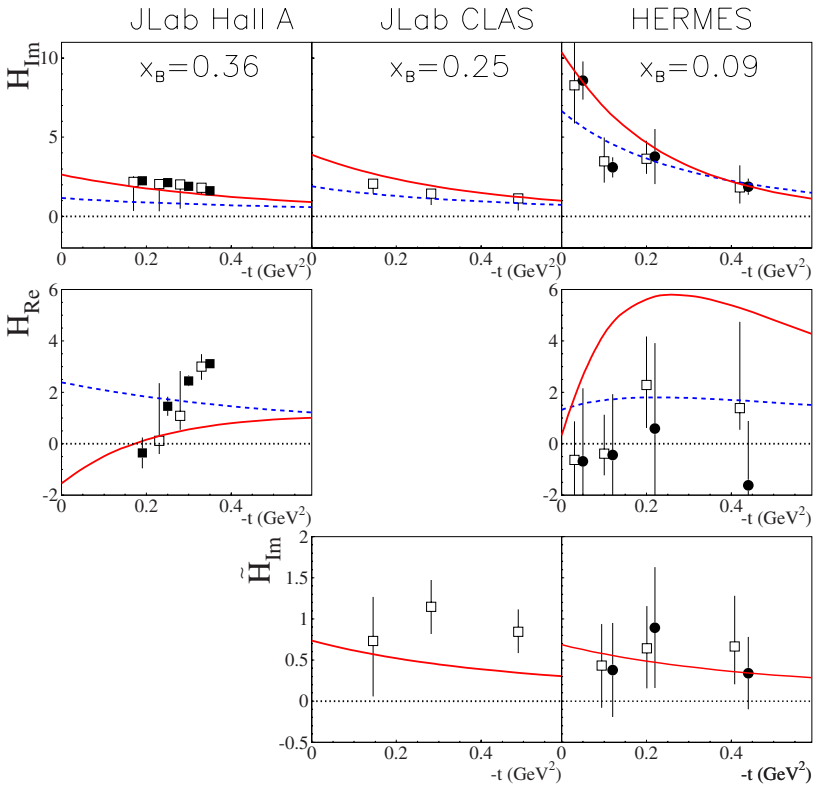

Figure 5. The H_{Im}, H_{Re} and $\tilde{H}_{Im}$ CFFs as a function of $-t$ for three different x_B values. The empty squares show the results of the 7 CFFs free parameters fit of Refs. [19–22]. The solid circles in the HERMES column show the result of the linear mapping fit of Ref. [17]. The solid squares in the JLab Hall A column show the result of the H-only CFF fit of Ref. [18]. The solid red curves show the result of the VGG model (with $b_{val} = b_{sea}$=1 and without any D-term for H) [1, 23–25]. The solid dashed blue curves show the results of the model-based fit of Ref. [16].

constraints obtained by the three groups mentioned above. Various fitting techniques have been used: "local", i.e. knowing the structure of the BH+DVCS amplitude, fitting in a quasi-model independent way the DVCS data at a given (x_B, Q^2, $-t$) kinematics, with the CFFs as free parameters; or "global", i.e. assuming a model-dependent functional shape for the (ξ, x, t)-dependence of the GPDs, fitting the parameters which enter the function, taking advantage of all DVCS data, over the whole (x_B, Q^2, $-t$) domain. In Fig. 5, we see the general good agreement of all fitting techniques, along with a couple of models.

Although uncertainties are rather large, some general features and trends can already be distinguished. For instance, the $t-$slope of H_{Im} seems to increase with x_B decreasing. We recall that the t-slope of the GPDs reflects, via a Fourier-type of transform, the electromagnetic charge spatial density of the nucleon. This t-slope evolution suggests that low-x quarks (the "sea") would extend to the periphery of the nucleon while the high-x (the "valence") would tend to remain in the center of the nucleon. In Ref. [4], a first attempt to quantify and visualize this change of the transverse size of the nucleon as lower longitudinal momentum fraction partons are probed was described. Using the CLAS and HERMES DVCS data presented in Sect. 2, via a Fourier-type of transform of the H_{Im} CFF and with a couple of model-dependent corrections, the contour plots of Fig. 6 were obtained.

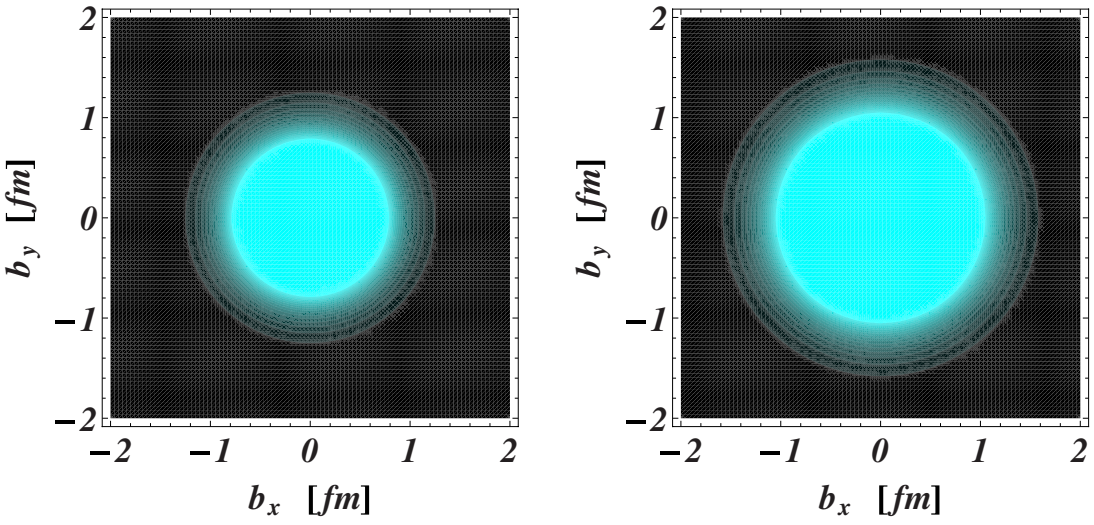

Figure 6. Left: contour plot of the transverse spatial charge density at CLAS kinematics (x_B=0.25). Right: contour plot of the transverse spatial charge density at HERMES kinematics (x_B=0.09).

In Fig. 5, the seemingly weaker t-dependence of $\tilde{H}_{Im}$ compared to H_{Im} also suggests that the axial charge (to which the $\tilde{H}$ GPD is related) has a narrower distribution in the nucleon than the electromagnetic charge.

4. Conclusion

In these proceedings, we have given a very brief overview of some of the latest developments in the field of GPDs, focusing on DVCS and on the valence region. We have shown how some new first 3-D information on the structure of the nucleon could be extracted from the data, thanks to the recent emergence of DVCS data fitting algorithms.

Several new experiments are planned and new data expected in the coming years at JLab 6 and 12 GeV and COMPASS which should provide soon stronger constraints on the extraction of GPDs and the 3D-imaging of the nucleon.

References

[1] K. Goeke, M.V. Polyakov and M. Vanderhaeghen, *Prog. Part. Nucl. Phys.* **47**, 401 (2001)
[2] M. Diehl, *Phys. Rept.* **388**, 41 (2003)
[3] A.V. Belitsky, A.V. Radyushkin, *Phys. Rept.* **418**, 1 (2005)
[4] M. Guidal, H. Moutarde and M. Vanderhaeghen, *Rept. Prog. Phys.* **76**, 066202 (2013)
[5] C. Muñoz Camacho et al., *Phys. Rev. Lett.* **97**, 262002 (2006)
[6] F.-X. Girod et al., *Phys. Rev. Lett.* **100**, 162002 (2008)
[7] S. Chen et al., *Phys. Rev. Lett.* **97**, 072002 (2006)
[8] A. Airapetian et al. [HERMES Collaboration], *Phys. Rev. Lett.* **87**, 182001 (2001)
[9] A. Airapetian et al. [HERMES Collaboration], *JHEP* **1207**, 032 (2012)
[10] A. Airapetian et al. [HERMES Collaboration], *JHEP* **1006**, 019 (2010)
[11] A. Airapetian et al. [HERMES Collaboration], *JHEP* **0806**, 066 (2008)

[12] A. Airapetian et al. [HERMES Collaboration], *Phys. Lett.* B **704**, 15 (2011)
[13] A. Airapetian et al. [HERMES Collaboration], *Phys. Rev.* D **75**, 011103 (2007)
[14] A. Airapetian et al. [HERMES Collaboration], *JHEP* **0911**, 083 (2009)
[15] A. Airapetian A. et al. [HERMES Collaboration], *Phys. Rev.* C **81**, 035202 (2010)
[16] K. Kumericki and D. Mueller, *Nucl. Phys.* B **841**, 1 (2010)
[17] K. Kumericki, D. Mueller and M. Murray, *Preprint* `arXiv:1302.7308 [hep-ph]` (2013)
[18] H. Moutarde, *Phys. Rev.* D **79**, 094021 (2009)
[19] M. Guidal, *Eur. Phys. J.* A **37**, 319 (2008). [Erratum-ibid. A **40**, 119 (2009)]
[20] M. Guidal and H. Moutarde, *Eur. Phys. J.* A **42**, 71 (2009)
[21] M. Guidal, *Phys. Lett.* B **689**, 156 (2010)
[22] M. Guidal, *Phys. Lett.* B **693**, 17 (2010)
[23] M. Vanderhaeghen, P.A.M. Guichon and M. Guidal, *Phys. Rev. Lett.* **80**, 5064 (1998)
[24] M. Vanderhaeghen, P.A.M. Guichon and M. Guidal, *Phys. Rev.* D **60**, 094017 (1999)
[25] M. Guidal, M.V. Polyakov, A.V. Radyushkin and M. Vanderhaeghen, *Phys. Rev.* D **72**, 054013 (2005)